Radiology: Cardiothoracic Imaging

ORIGINAL RESEARCH

Characterizing Lung Parenchymal Aeration via Standardized Signal Intensity from Free-breathing 4D Dynamic MRI in Phantoms, Healthy Children, and Pediatric Patients with Thoracic Insufficiency Syndrome

Yubing Tong, PhD • Jayaram K. Udupa, PhD • Joseph M. McDonough, MS • Caiyun Wu, MS • Lipeng Xie, PhD • Chamith S. Rajapakse, PhD • Samantha Gogel, BA • Sulagna Sarkar, MS • Oscar H. Mayer, MD • Jason B. Anari, MD • Drew A. Torigian, MD, MA • Patrick J. Cahill, MD

From Department of Radiology, the Medical Image Processing Group, University of Pennsylvania, 3710 Hamilton Walk, Goddard Bldg, 6th Fl, Philadelphia, PA 19104 (Y.T., J.K.U., C.W., L.X., D.A.T.); The Wyss/Campbell Center for Thoracic Insufficiency Syndrome, The Children's Hospital of Philadelphia, Philadelphia, Pa (J.M.D., S.G., S.S., J.B.A., P.J.C.); Departments of Radiology and Orthopedic Surgery, University of Pennsylvania, Philadelphia, Pa (C.S.R.); and Division of Pulmonology, The Children's Hospital of Philadelphia, Philadelphia, Pa (O.H.M.). Received September 7, 2023; revision requested October 13; revision received May 2, 2024; accepted May 31. **Address correspondence to** J.K.U. (email: *jay@pennmedicine.upenn.edu*).

Supported by the National Institutes of Health (grant no. R01HL150147).

Conflicts of interest are listed at the end of this article.

Radiology: Cardiothoracic Imaging 2024; 6(4):e230262 • https://doi.org/10.1148/ryct.230262 • Content codes: CH MR PD

Purpose: To investigate free-breathing thoracic bright-blood four-dimensional (4D) dynamic MRI (dMRI) to characterize aeration of parenchymal lung tissue in healthy children and patients with thoracic insufficiency syndrome (TIS).

Materials and Methods: All dMR images in patients with TIS were collected from July 2009 to June 2017. Standardized signal intensity (sSI) was investigated, first using a lung aeration phantom to establish feasibility and sensitivity and then in a retrospective research study of 40 healthy children (16 male, 24 female; mean age, 9.6 years ± 2.1 [SD]), 20 patients with TIS before and after surgery (11 male, nine female; mean age, 6.2 years ± 4.2), and another 10 healthy children who underwent repeated dMRI examinations (seven male, three female; mean age, 9 years ± 3.6). Individual lungs in 4D dMR images were segmented, and sSI was assessed for each lung at end expiration (EE), at end inspiration (EI), preoperatively, postoperatively, in comparison to normal lungs, and in repeated scans.

Results: Air content changes of approximately 6% were detectable in phantoms via sSI. sSI within phantoms significantly correlated with air occupation (Pearson correlation coefficient = −0.96 [$P < .001$]). For healthy children, right lung sSI was significantly lower than that of left lung sSI (at EE: 41 ± 6 vs 47 ± 6 and at EI: 39 ± 6 vs 43 ± 7, respectively; $P < .001$), lung sSI at EI was significantly lower than that at EE ($P < .001$), and left lung sSI at EE linearly decreased with age ($r = -0.82$). Lung sSI at EE and EI decreased after surgery for patients (although not statistically significantly, with P values of sSI before surgery vs sSI after surgery, left and right lung separately, in the range of 0.13–0.51). sSI varied within 1.6%–4.7% between repeated scans.

Conclusion: This study demonstrates the feasibility of detecting change in sSI in phantoms via bright-blood dMRI when air occupancy changes. The observed reduction in average lung sSI after surgery in pediatric patients with TIS may indicate postoperative improvement in parenchymal aeration.

Supplemental material is available for this article.

Thoracic insufficiency syndrome (TIS) is the inability of the thorax to support normal breathing or lung growth (1,2). It is vital to study lung parenchymal aeration to understand lung physiologic status before and after treatment for TIS (3). Current lung parenchymal aeration characterization via CT (4), hyperpolarized gas MRI (5–9), or single-plane two-dimensional (2D) dynamic MRI (dMRI) (10) may not be feasible in clinical practice; possible reasons include radiation concerns (4), difficulties in practical clinical implementation (5,6), or the need for patient cooperation, such as breath holding (10,11) or use of a spirometer during breathing (12), which cannot be implemented for routine use in all patient groups, especially pediatric patients.

Fourier decomposition MRI strategies for assessing lung ventilation focus on the region inside the lungs and perform only 2D analyses (13,14). Ultrashort echo time (UTE) techniques have been used to quantify perfusion in lung parenchyma (15), and respiratory-gated UTE sequences have been used to measure lung tissue density (16), both only in animal studies. Phase-resolved functional lung (PREFUL) MRI (17–19) seems to enable ventilation measurement with free breathing. However, it has been demonstrated only in adults (18,19). Three-dimensional (3D) PREFUL images have low resolution and a voxel size of 4 × 4 × 4 mm^3 (17), and 2D PREFUL images have a large section spacing of 15 mm (18,19), posing challenges for image segmentation and analysis. Furthermore, image acquisition time is approximately 1 hour per individual (17), which is impractical for routine clinical use.

The images for patients with TIS can be obtained practically during free breathing with short image

Abbreviations

dMRI = dynamic MRI, EE = end expiration, EI = end inspiration, 4D = four-dimensional, PREFUL = phase-resolved functional lung, sSI = standardized signal intensity, TIS = thoracic insufficiency syndrome, 3D = three-dimensional, 2D = two-dimensional, UTE = ultrashort echo time, VEPTR = vertical expandable prosthetic titanium rib

Summary

This study provides a practical and sensitive approach via commonly available bright-blood dynamic MRI to measure lung parenchymal aeration in pediatric patients to assess lung disease severity and treatment effects.

Key Points

- Air content changes of 6.25% were detectable in lung aeration phantoms via standardized signal intensity (sSI) in bright-blood dynamic MRI, and sSI measurement was highly repeatable.
- For healthy children, sSI of the right lung was significantly lower than that of the left lung at end expiration (EE) (41 ± 6 vs 47 ± 6) and end inspiration (EI) (39 ± 6 vs 43 ± 7) ($P < .001$), and sSI at EI was significantly lower than that of EE for both lungs ($P < .001$).
- sSI at EE and EI showed a nonsignificant decrease after surgery for patients with thoracic insufficiency syndrome (with P values of sSI before surgery vs sSI after surgery, left and right lung separately, in the range of .13–.51).

Keywords

MR Imaging, Thorax, Lung, Pediatrics, Thoracic Surgery, Lung Parenchymal Aeration, Free-breathing Dynamic MRI, MRI Intensity Standardization, Thoracic Insufficiency Syndrome

acquisition time and high spatial resolution. A quantitative dMRI technique was previously developed to measure lung dynamics in terms of volumes and tidal volumes and demonstrated its use in TIS treatment planning and evaluation (20–23). The primary aim of the current study was to investigate if the same dMRI sequence can also be used to measure parenchymal aeration. This bright-blood dMRI technique achieves a much higher spatial resolution of approximately 1 × 1 × 6 mm^3 as compared with PREFUL MRI (19), with a much shorter acquisition time of 15–20 minutes (19–22).

In this retrospective case-control study, we evaluated whether changes in air content in individual lungs from end expiration (EE) to end inspiration (EI) and from preoperative to postoperative conditions were detectable via dMRI standardized signal intensity (sSI). sSI values are derived from four-dimensional (4D) constructed dMR images by using intensity standardization techniques, which enable the MR intensity values to have the specific tissue meaning across all individuals (26). Some preliminary results have been published in an earlier conference paper (24). This work substantially extends that paper by using a cohort that is twice as large, adding a phantom experiment for validation and additional healthy children for repeatability evaluation, providing methods in greater detail, and presenting a complete analysis of the results.

Materials and Methods

Phantoms, Study Cohorts, and Image Data Sets

All data were acquired under an ongoing research protocol approved by the institutional review boards at our institutions, along with a Health Insurance Portability and Accountability Act waiver. The requirement for patient consent was waived by the institutional review boards. The study included 40 healthy children and 20 patients with TIS with 40 thoracic dMRI-acquired scans before and after vertical expandable prosthetic titanium rib (VEPTR) surgical treatment (25,35). Ten patients with TIS with their 20 thoracic dMRI scans were reported in our previous work (24). VEPTR is a U.S. Food and Drug Administration–approved TIS treatment approach where expandable titanium ribs are implanted into a child's back and chest and anchored to the spine and ribs (25). The diagnosis of TIS was based on multiple components, including history, physical examination, radiographs, and imaging techniques such as CT or MRI, as well as pulmonary function testing. Often, skeletal dysplasia will produce clear respiratory or growth limitations, but having skeletal deformity in and of itself is not sufficient to make the diagnosis of TIS (35–38). Pediatric patients not diagnosed with TIS or with insufficient clinical or radiographic data were excluded. Another 10 healthy children were included for evaluating the repeatability of sSI by scanning them twice with a short interval between scans. Figure 1 shows the patient inclusion/exclusion flowchart.

The aeration phantom consisted of seven well-sealed polyvinyl acetate sponge blocks (Simplygoodstuff.com) of identical size (8.5 × 7.0 × 3.0 cm^3). The air content of the blocks was adjusted by displacement with water and expressed as a ratio of air in block (in milliliters) to volume of block, ranging from 0.5 to 0.8 in increments of 0.05 among the seven blocks, as depicted in Figure 2.

dMRI Acquisition

For the cohorts, the details of the thoracic dMRI protocol are as follows: 3-T MRI scanner (Verio; Siemens), true fast imaging with steady-state precession sequence, repetition time of 3.82 msec, echo time of 1.91 msec, voxel size of approximately 1 × 1 × 6 mm^3, 320 × 320 matrix, bandwidth of 258 Hz, and flip angle of 76°. For each sagittal location across the thorax, 40 2D sections were acquired over several tidal breathing cycles at approximately 480 msec/section. On average, 35 sagittal locations were imaged, yielding a total of approximately 1400 2D sections, within a scan time of 11–13 minutes (22).

The phantom was scanned using the same dMRI protocol. Each "sagittal" section contained a cross-section of all seven blocks, where a total of 15 sections were acquired across the phantom, and each section location was continuously/repeatedly scanned 40 times.

Image Processing Operations

For each dMRI scan, an automated 4D image construction approach was used (20) to form one 4D image of the thorax over one breathing cycle consisting of typically five to eight

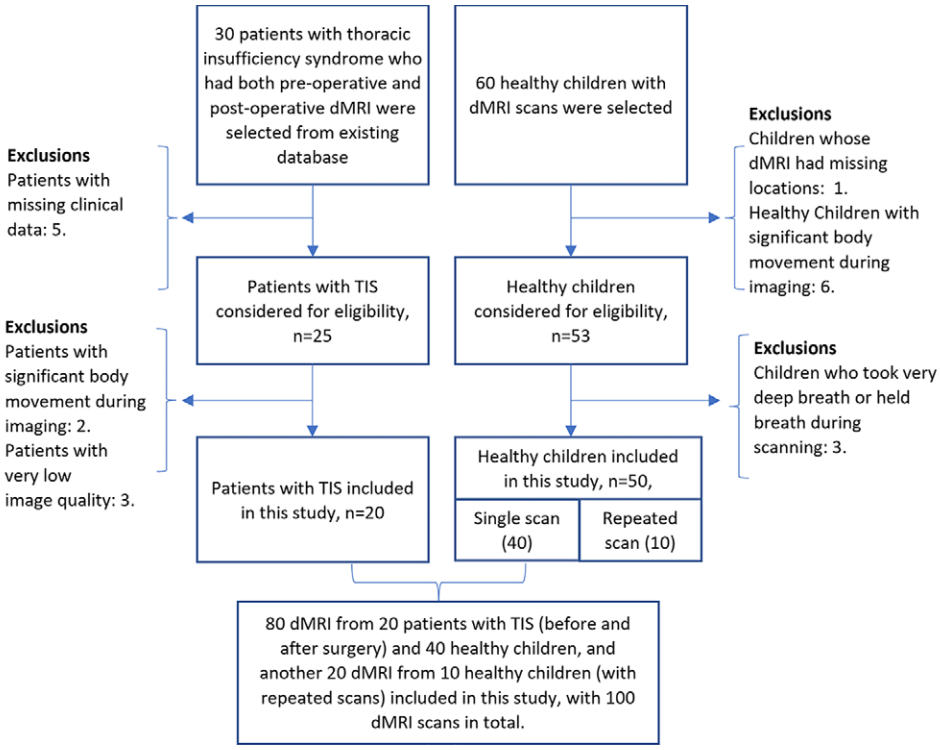

Figure 1: Patient inclusion and exclusion flowchart. dMRI = dynamic MRI, TIS = thoracic insufficiency syndrome.

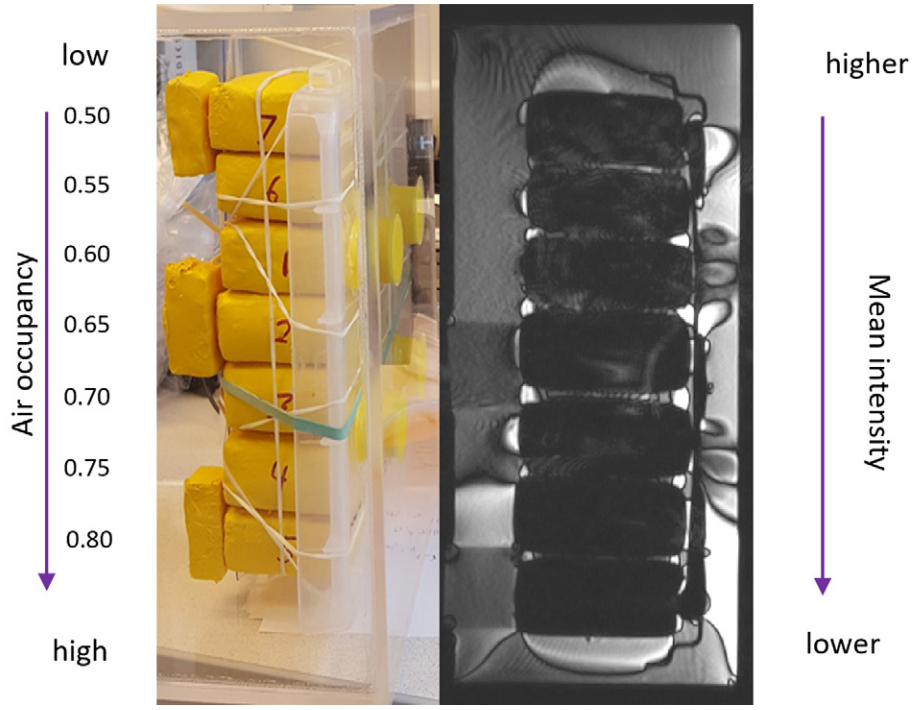

Figure 2: Photograph and bright-blood MRI scan of lung aeration phantom. The air occupancy in blocks is depicted as the ratio of the volume of air to the volume of block, with a range of 0.50–0.80 from block 7 to block 5 (top to bottom, with 0.05 difference between blocks). Mean signal intensity in blocks decreases (appears darker) with increasing air occupancy.

respiratory phases and roughly 175–280 sections (35 sagittal locations × five to eight respiratory phases). For the phantom, no 4D construction was required because it is static, and the repeatedly acquired sections helped to improve sSI statistics.

Intensity standardization is a well-established postacquisition nonlinear image transform technique that is applied to the 4D constructed image to provide sSI values (26) so that similar tissues will have similar numeric values.

Table 1: Characteristics of Study Cohort

Parameter	Dynamic MRI in Patients with Thoracic Insufficiency Syndrome			Dynamic MRI in Healthy Controls	Repeated Dynamic MRI in Healthy Controls
	Preop Group (n = 20)	Postop Group (n = 20)	P Value (Preop Group vs Postop Group)		
Sex	9 F, 11 M	9 F, 11 M		24 F, 16 M	3 F, 7 M
Age (y)	5.4 ± 4.3	7.1 ± 4.1	.19	9.6 ± 2.1	10.9 ± 3.6
Height (cm)	94.5 ± 28.8	109.6 ± 26.9	.09	133.6 ± 13.9	145.3 ± 21.2
Weight (kg)	17.1 ± 10.7	21.1 ± 10.2	.22	33.8 ± 11.2	41.6 ± 15.5

Note.—Unless otherwise noted, data are reported as means ± SDs. A total of 40 dynamic MRI examinations were performed in 20 patients with thoracic insufficiency syndrome. A total of 40 initial dynamic MRI examinations were performed in 40 healthy controls, and 20 repeat MRI examinations were performed in 10 healthy controls. Postop = postoperative, Preop = preoperative.

For lung segmentation, a pretrained U-Net–based deep learning network was used to segment each lung in the intensity-standardized 4D image. It yielded a mean Dice coefficient for segmentation of 0.97 ± 0.02 (SD) (27). Segmentations were manually refined, as needed, under the supervision of a radiologist (D.A.T.) with 25 years of expertise in MRI and thoracic radiology.

Deriving sSI Properties

For phantoms, rectangular regions of interest were selected in each section to fully cover the block but exclude edges of the blocks where MRI artifacts are typically observed. For each block, the mean ± SD of sSI within the region of interest was estimated over all sections.

For patients with TIS and healthy children, the mean ± SD of sSI within the aerated portions of the lungs was estimated using the segmented lung mask. These aerated portions were obtained by setting a threshold to exclude regions corresponding to large pulmonary veins and arteries and nonaerated lung tissue, under supervision of a board-certified radiologist (D.A.T.). This was rather straightforward because lung tissue has much lower signal intensity than other tissues within the mask. The mean ± SD sSI was determined over the whole 3D lung mask after excluding large blood vessels. To determine the operator-dependent variability of sSI, two operators (C.W., Y.T.) with extensive experience with dMRI and lung segmentation performed this step for capturing aerated portions of the left and right lungs in five healthy children and five patients with TIS at EE and EI. sSI values from the two operators were compared via a paired t test. Additionally, sSI values and lung volumes from the repeated scans were measured, and the repeatability of those measurements was assessed via paired t testing.

Statistical Analysis of sSI

The statistical toolbox in MATLAB (R2019b; MathWorks) was used. Pearson correlation analysis was performed to study the association between phantom sSI and known air content. Two-sided paired t testing was performed to compare the mean sSI among blocks taken in pairs.

Pearson correlation analysis was performed to estimate the association between sSI and volumetric measurements. Two-sided paired t testing was performed to compare sSI at EE and EI for healthy children and patients with TIS preoperatively and postoperatively. Comparisons of sSI between patients with TIS and healthy children were also performed. In all comparisons, P values less than .05 indicated a statistically significant difference.

Results

Cohort Characteristics

Table 1 summarizes the basic characteristics of 40 healthy children (single scan), 10 healthy children (repeated scans), and 20 patients with TIS (preoperatively and postoperatively). Patients with TIS included nine female and 11 male patients with a mean age of 5.4 years ± 4.3 preoperatively and 7.1 years ± 4.1 postoperatively, and healthy children included 24 female and 16 male children with a mean age of 9.6 years ± 2.1. Ten healthy children who underwent repeated scans included three female and seven male children with a mean age of 10.9 years ± 3.6. Both qualitative and quantitative study results are reported below.

Qualitative Results

Figure 2 shows the phantom and its associated MRI scan. The intensities within the blocks were visually confirmed to appear darker with increasing air content. For the seven blocks, all 21 possible pairwise comparisons of the blocks indicated that the mean sSI differed significantly among blocks ($P < .001$), even between blocks 5 and 4, with the smallest percentage difference in aeration ratio of 0.05/0.8 = 6.25%. All 40 repeated scans behaved similarly. The Pearson correlation coefficient between sSI and air occupancy over the seven blocks was −0.96 ($P < .001$).

Figure 3 illustrates sagittal dMR images before and after intensity standardization with the same grayscale display range being set up relative to the middle column image. After intensity standardization, similar tissue types from a patient with TIS and a healthy child have more similar intensity ranges and can be displayed for proper visualization using the same display range.

Figure 4 shows an example of segmented aerated lungs (right and left lungs, separately) at dMRI at EE and EI in one male patient with TIS and in one healthy male child of a similar age. The lung sSI is overlaid in color over the MRI section where

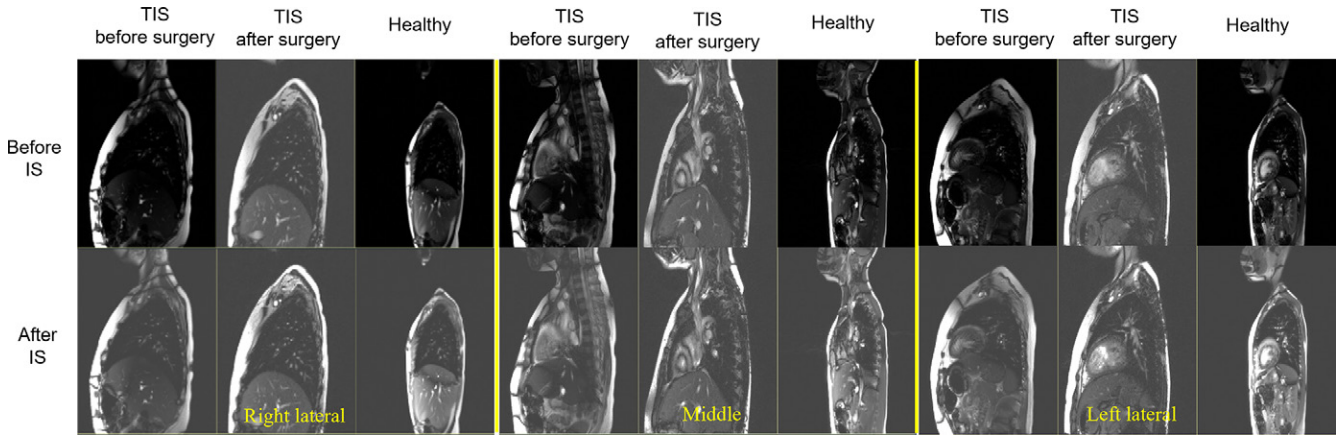

Figure 3: Intensity standardization (IS) of dynamic MRI (dMRI) scans in two individuals: a patient with TIS before surgery (first, fourth, and seventh columns), the same patient with TIS after surgery (second, fifth, and eight columns), and one healthy control (third, sixth, and ninth columns). Sagittal dMR images in three locations through the thorax (first through third columns: right lateral, fourth through sixth columns: middle, seventh through ninth columns: left lateral) are shown for both individuals. The grayscale display range is set up for display relative to the middle column image. The top row shows images before IS and the bottom row for images after IS. TIS = thoracic insufficiency syndrome.

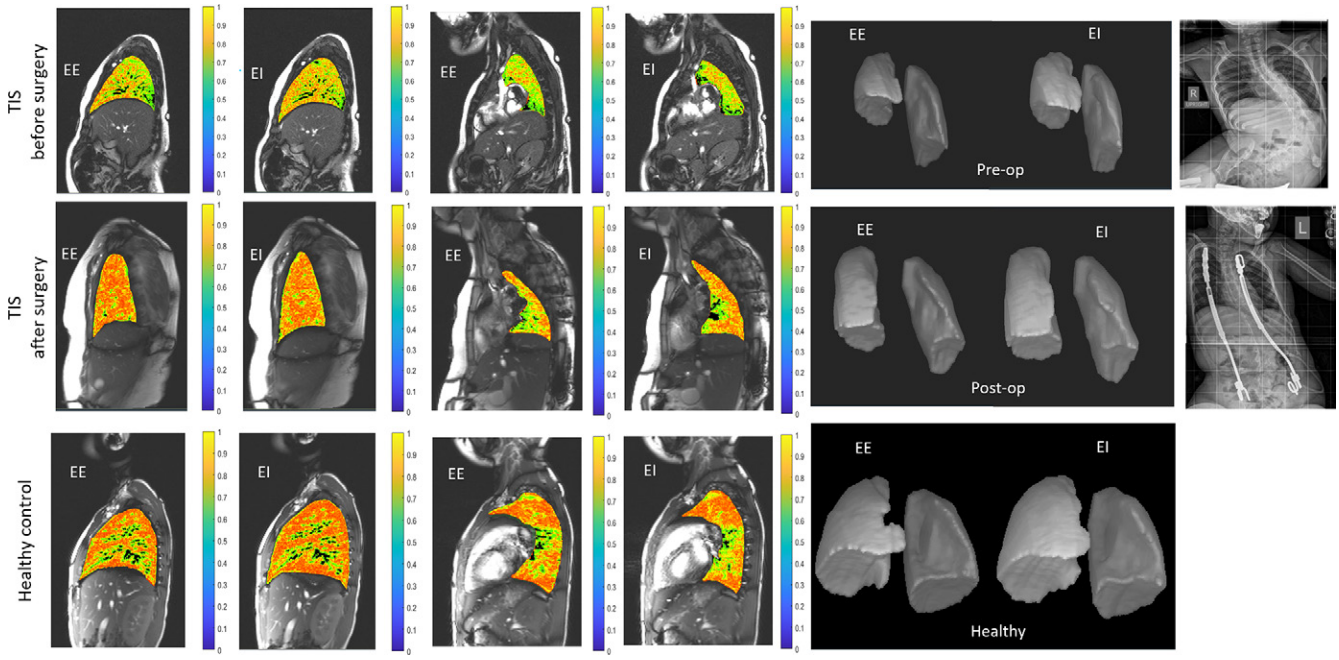

Figure 4: A representative example of aerated lungs on two-dimensional sagittal MR images at EE and EI and three-dimensional lung surface renditions at EE and EI in one patient with TIS before surgery (top row, 6.5-year-old male patient), the same patient with TIS after surgery (middle row, 9.2-years old), and one healthy control (bottom row, 7.9-year-old male child). Color maps of sSI are shown overlaid on dynamic MRI sections, with yellower and redder colors indicating lower sSI or greater aeration. EE = end expiration, EI = end inspiration, sSI = standardized signal intensity, TIS = thoracic insufficiency syndrome.

deeper yellow and red indicate lower sSI or greater aeration. We observed that the volume of the lungs at EI becomes larger than that at EE, sSI at EI in all instances becomes lower than that at EE, and sSI at both EE and EI decrease after surgery.

Figure 5 illustrates the linear correlation analysis between lung mean sSI and age in healthy children, demonstrating that sSI appears to decrease with increasing age, with slope coefficients in the range of −0.82 to −0.55. The relationship between sSI and age for the left lung (at EE and EI) has a greater slope than that for the right lung.

Figure S1 shows the original dMR image and the color map of sSI overlaid on dMRI sections, with yellower and redder colors indicating lower sSI or greater aeration, for one healthy child (female, 8.2 years). Two video files depicting the animations of the dMRI original intensity and sSI overlaid as a color map over one respiratory cycle for the same healthy child are provided (Movies 1, 2).

Quantitative Results

Table 2 summarizes statistics of sSI and aerated volumes of lungs at EE and EI for healthy children and Pearson correlation coefficients between sSI and volumes. A very strong correlation (r = 0.85–0.92) was found between left and right lung sSI at both EE and EI, although right lung sSI was significantly lower

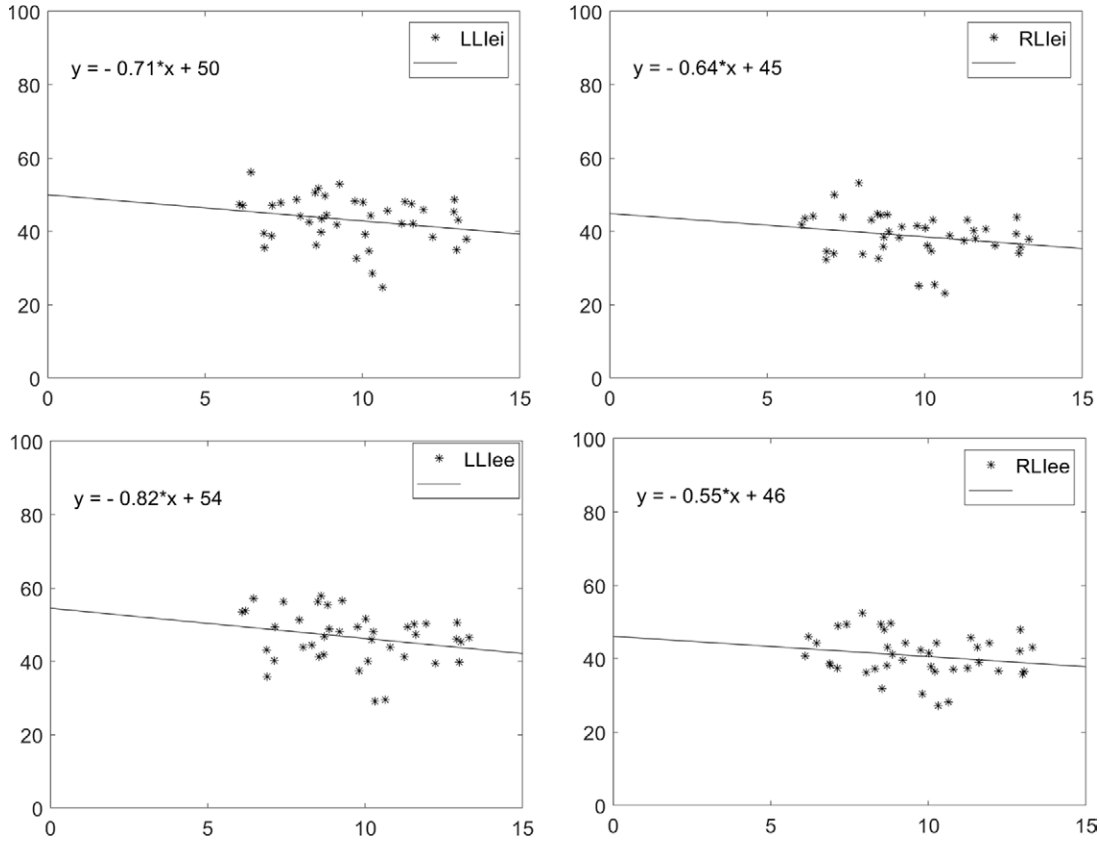

Figure 5: Linear correlations between standardized signal intensity (sSI) (vertical axis) and age in years (horizontal axis) in healthy children for left and right lungs at end inspiration (EI) and end expiration (EE). LLlee = left lung signal intensity at EE, LLlei = left lung signal intensity at EI, RLlee = right lung signal intensity at EE, RLlei = right lung signal intensity at EI.

(P < .001) than left lung sSI at both EE and EI. Although aerated volumes were strongly correlated between left and right lungs (r = 0.95–0.97), sSI showed poor negative correlation (r = −0.08 to −0.20) with lung volumes at EE and EI for both lungs over all healthy children. Similarly, the change of sSI from EE to EI showed nonsignificant negative correlation with volume change from EE to EI. These negative correlations (for sSI and lung volumes) changed to between −0.41 and −0.64 for healthy children younger than 8 years but approached zero for healthy children older than 8 years.

Table 3 summarizes aerated lung sSI and volumes at EE and EI for patients with TIS preoperatively and postoperatively. sSI from the preoperative group behaved the same way as sSI from the postoperative group when comparing EE and EI or comparing left lung versus right lung within each group. sSIs in EE and EI showed a behavior similar to those in healthy children in terms of how sSI values compared and correlated. sSI at EE and EI decreased, though not significantly, after surgery for patients with TIS, indicating improved lung aeration. The aerated lung volumes (EE and EI, left and right lungs) also showed a nonsignificant decrease after surgery. Age-corrected sSI (and aerated volumes) for patients with TIS was obtained by first fitting a linear function to sSI (and aerated volumes) of healthy children as a function of age and then using this function to estimate, by extrapolation, what the preoperative sSI value (aerated volume) would be for the patient at the postoperative age. For example, the function obtained for sSI for left lung at EI (Fig 5) was sSI(x) = −0.82x + 54.

Table 4 demonstrates the repeatability of sSI and shows no evidence of a difference in the mean sSI of the aerated lungs estimated by two operators (with P values of .22 to .67). The difference in sSI was 1.6%–4.7%, with all P values less than .05 for EE (P values of .35 and .42 for patients with TIS and healthy children, respectively) and EI (P values of .67 and .42 for patients with TIS and healthy children, respectively). Table 5 demonstrates the high repeatability of the sSI measurement from repeated dMRI scans. No evidence of differences was observed in sSI at either EE or EI between the repeated scans (P > .05). The experiments also showed a high repeatability of lung volumes obtained from repeated dMRI scans, with volume differences of 1.7% and 2.1% for EI and EE, respectively (P > .05). To study the variation of sSI and repeatability of sSI in different regions of the lungs, each lung was split into three regions—superior third, middle third, and inferior third—and sSI was estimated in these regions in the repeated scans. The results demonstrated that sSI in the superior region was significantly lower than sSI in the middle and inferior regions (Table 6, all P values < .001 of superior region vs middle region). Across the repeated scans, there was no evidence of a difference in repeated sSI measurements for each region (all P values in the range of .38–.97).

Furthermore, by using a linear mixed model with patient random effects, we found a significant decrease in mean sSI of 10.12

Table 2: Standardized Signal Intensity and Volume of Left and Right Aerated Lungs at End Expiration and End Inspiration for 40 Healthy Pediatric Controls

Parameter	Aerated Lung sSI	Aerated Lung Volume
LL at EI	43 ± 7	427.2 ± 134.6*
RL at EI	39 ± 6	564.6 ± 161.1*
LL at EE	47 ± 7	346.5 ± 122.5*
RL at EE	41 ± 6	462.5 ± 143.7*
Paired *t* test, RL vs LL		
P value, LL at EI vs RL at EI	<.001	<.001
P value, LL at EE vs RL at EE	<.001	<.001
Paired *t* test, EI vs EE		
P value, LL at EI vs LL at EE	<.001	<.001
P value RL at EI vs RL at EI	<.001	<.001
Pearson correlation coefficients		
LL at EI vs LL at EE	0.92	0.97
RL at EI vs RL at EE	0.92	0.99
LL at EI vs RL at EI	0.85	0.95
LL at EE vs RL at EE	0.86	0.97
LL at EI†	−0.16	
RL at EI†	−0.12	
LL at EE†	−0.20	
RL at EE†	−0.08	
LL at EE and EI†	−0.29	
RL at EE and EI†	−0.17	
FRC of LL at EE†	−0.07	
FRC of RL at EE†	−0.15	
sSI of LL at EE vs volume of BL at EE	−0.21	
sSI of RL at EE vs volume of BL at EE	−0.07	
FRC of volume of BL at EE	0.48	

Note.—Means ± SDs of sSI and aerated lung volume are shown, as well as Pearson correlation coefficients among sSIs, among volumes, and between sSI and volume. Among 40 healthy children, functional residual capacity (FRC) assessment from pulmonary function testing was available for only 24 children. BL = both lungs, EE = end expiration, EI = end inspiration, LL = left lung, RL = right lung, sSI = standardized signal intensity.
* Lung volume presented in milliliters.
† Pearson correlation coefficient is comparing sSI versus volume for the given parameter.

(*P* = .01) from before to after surgery and a significant mean difference of 11.14 (*P* = .006) between expiration and inspiration. Left versus right lung, as well as interaction terms, were considered but none were statistically significant. These findings are also supported using a two-way analysis of variance model.

Discussion

We developed a method to estimate lung aeration at dMRI based on an aeration phantom and assessed its utility on 40 thoracic dMRI scans in 20 patients with TIS (before and after surgery), 40 dMRI scans in healthy children, and 20 repeated dMRI scans in healthy children. We observed that the average sSI of the lung at EI was significantly lower than that at EE (43 ± 7 at EI vs 47 ± 7 at EE for left lung and 39 ± 6 at EI vs 41 ± 7 at EE for right lung, with both *P* values < .001) in healthy children and had similar observations for patients with TIS, indicating an inverse association between lung air occupancy and lung sSI. Additionally, the sSI of the right lung (before surgery: 61 ± 22, after surgery: 63 ± 21) was significantly lower than that of the left lung (before surgery: 71 ± 26, *P* = .007; after surgery: 57 ± 23, *P* = .02) at EI, although the sSIs of the two lungs were highly correlated (with preoperative correlations of 0.81 and 0.83 for EI and EE, respectively, and postoperative correlations of 0.90 and 0.95 for EI and EE, respectively). Lung sSI in patients with TIS (before and after surgery) showed moderate negative correlations (−0.52 to −0.27) with aerated lung volumes. Lung sSI at EE of patients with TIS before and after surgery did not significantly differ, suggesting that surgical intervention has a greater influence on lung aeration during inspiration than at resting volume.

Electrical impedance tomography, a noninvasive and real-time technique, permits assessment of physiologic and potential

Table 3: Standardized Signal Intensity and Volume of Left and Right Aerated Lungs at End Expiration and End Inspiration for 20 Patients with TIS

A: Before Surgery

Parameter	Aerated Lung sSI	Aerated Lung Volume
LL at EE	79 ± 32	348.4 ± 302.8*
RL at EE	73 ± 30	489.9 ± 485.1*
LL at EI	71 ± 26	429.5 ± 355.2*
RL at EI	61 ± 22	601.6 ± 537.3*
Paired *t* test, RL vs LL		
P value, RL at EE vs LL at EE	.14	.02
P value, RL at EI vs LL at EI	.007	.03
Paired *t* test, EI vs EE		
P value, LL at EI vs LL at EE	.002	<.001
P value, RL at EI vs RL at EE	<.001	<.001
Correlation		
LL at EI vs RL at EI		
PC	0.81	0.91
P value	.1	.02
LL at EE vs RL at EE		
PC	0.83	0.82
P value	.007	.03
PC, LL at EE†	−0.52	
PC, LL at EI†	−0.47	
PC, RL at EE†	−0.50	
PC, RL at EI†	−0.47	

B: After Surgery

Parameter	Aerated Lung sSI	Aerated Lung Volume
LL at EE	69 ± 24	388.7 ± 239.3*
RL at EE	65 ± 21	565.8 ± 353.9*
LL at EI	57 ± 23	497.5 ± 258.2*
RL at EI	53 ± 21	726.9 ± 394.0*
Paired *t* test, RL vs LL		
P value, RL at EE vs LL at EE	.09	<.001
P value, RL at EI vs LL at EI	.02	<.001
Paired *t* test, EI vs EE		
P value, LL at EI vs LL at EE	<.001	<.001
P value, RL at EI vs RL at EE	.002	<.001
Correlation		
LL at EI vs RL at EI		
PC	0.90	0.92
P value	.10	<.001
LL at EE vs RL at EE		
PC	0.95	0.84
P value	.02	<.001
LL at EE†	−0.40	
LL at EI†	−0.45	
RL at EE†	−0.27	
RL at EI†	−0.35	

(Table 3 continues)

Table 3 *(continued)*: Standardized Signal Intensity and Volume of Left and Right Aerated Lungs at End Expiration and End Inspiration for 20 Patients with TIS

C: Before Surgery vs after Surgery‡

Parameter	Preoperative sSI, Age Corrected	Preoperative Aerated Lung Volume, Age Corrected
LL at EE	73 ± 34	490.0 ± 365.0*
RL at EE	69 ± 32	642.3 ± 547.0*
LL at EI	66 ± 28	579.2 ± 422.2*
RL at EI	56 ± 23	768.0 ± 604.6*
P value, LL at EE	.51	.08
P value, RL at EE	.5	.32
P value, LL at EI	.13	.27
P value, RL at EI	.48	.64

Note.—Means ± SDs of sSI and aerated lung volume are reported, as well as *P* values from paired *t* tests. Pearson correlation coefficients (PCs) are also listed for sSI and volume. EE = end expiration, EI = end inspiration, LL = left lung, RL = right lung, sSI = standardized signal intensity, TIS = thoracic insufficiency syndrome.
* Lung volume presented in milliliters.
† Values are comparing sSI and volume.
‡ Comparisons made using paired *t* test.

Table 4: Comparisons of Standardized Signal Intensity of Aerated Lungs at End Expiration and End Inspiration in Patients with TIS and Healthy Controls

	Patients with TIS		Healthy Controls	
Parameter	EI	EE	EI	EE
Operator 1	64 ± 27	79 ± 24	43 ± 4	46 ± 6
Operator 2	65 ± 25	77 ± 21	41 ± 4	48 ± 6
P value, operator 1 vs operator 2	.67	.35	.22	.42

Note.—A total of 10 lungs in five patients with TIS and 10 lungs in five healthy controls were compared. Values were measured by two operators. Means ± SDs of standardized signal intensity are reported, along with *P* values from paired *t* test comparisons. EE = end expiration, EI = end inspiration, TIS = thoracic insufficiency syndrome.

Table 5: Comparisons of Standardized Signal Intensity and Lung Volume at End Expiration and End Inspiration from Repeated Scans in Healthy Controls

	sSI			Lung Volume Difference (%)	
Parameter	EI	EE	*P* Value, EI vs EE	EI	EE
First scan	36 ± 5	40 ± 7	.001	1.74 ± 1.23	2.13 ± 1.55
Second scan	36 ± 7	40 ± 8	.01		
P value, first vs second scan	.67	.65	…	.83	.51

Note.—A total of 20 repeated scans were performed in 10 healthy controls. Means ± SDs of sSI are reported, along with *P* values from paired *t* test comparisons. Lung volume difference is calculated as $(V_{first} - V_{second})/V_{first}$, where V_{first} is the volume at the first scan and V_{second} is the volume at the second scan. EE = end expiration, EI = end inspiration, sSI = standardized signal intensity.

Table 6: Standardized Signal Intensity to Characterize Parenchyma within Three Lung Portions on Repeated Scans of Single Lung in Healthy Controls

Parameter	S	M	I	*P* Value, S vs M	*P* Value, S vs I	*P* Value, M vs I
First scan						
EE	28 ± 8	44 ± 11	40 ± 8	<.01	.002	.12
EI	24 ± 4	38 ± 7	38 ± 6	<.001	<.001	.87
P value, EE vs EI	.024	.004	.034	…	…	…
Second scan						
EE	29 ± 8	44 ± 10	41 ± 9	<.001	.001	.2
EI	26 ± 8	39 ± 8	37 ± 7	<.001	.003	.54
P value, EE vs EI	.03	.01	.01	…	…	…
P value, first scan vs second scan						
EE	.58	.97	.55	…	…	…
EI	.38	.63	.54	…	…	…

Note.—Means ± SDs of sSI are reported, along with *P* values from paired *t* test comparisons. Parenchyma was characterized in superior (S), middle (M), and inferior (I) lung portions on 20 repeated scans of a single lung in 10 healthy controls. Repeated scans include first and second scans. EE = end expiration, EI = end inspiration, sSI = standardized signal intensity.

pathophysiologic evolutions, such as the evolution of a tumor. In the study by Zhang et al (29), this technique has been used to detect changes in lung parenchymal aeration but was evaluated only in a few (eight total) adults with scoliosis. Other methods have assessed the change in air content in lungs at only a few sections/locations, as in the studies by Tibiletti et al (15) and Burjek et al (30). The study by Zapke et al (31) is perhaps the one closest to our study, which showed a high correlation (r = 0.8) between MR image–based ventilation volumes and forced vital capacity. However, it used dynamic MRI in a single coronal plane corresponding to the middle section through the two lungs for estimation of local ventilation based on several assumptions, including an assumed model of the shape of the lungs. A ratio factor of the intensity change at every time point to the reference intensity at expiration was defined to reflect the volume change, and the volumes of the entire lungs were then estimated by using lung volumes from static MRI multiplied by that ratio factor. Six sample regions of interest were manually placed within the lung at different respiratory phases to estimate the intensity change. Our method is fully 3D, dynamic (truly 4D), and, we believe, more practical and realistic for pediatric patients than that presented in Zapke et al (31) or any other existing approaches (39,40). It does not make any assumptions about lung shape or pattern of intensity change; such assumptions may be invalid in the case of patients with TIS and patients with other disorders. Our approach simply measures the volume and intensity parameters directly from acquired true 4D imagery of the full thorax under free-breathing conditions without any requirements for specific breathing maneuvers. Another potential issue for the method in Zapke et al (31) is the large section thickness of 60 mm (vs 6 mm in our study). A previous study reported quantification of lung parenchymal density via UTE MRI with comparison to CT (41), where MR images were acquired in the free-breathing condition and then retrospective respiratory self-gating (42) was used to build the image at EE and EI. All experiments in two studies by Higano et al (41,42) were performed by using adult data, and the lungs were segmented manually. Their focus was on comparing the mean lung intensity at UTE MRI after normalizing it to the muscle intensity at CT. However, the comparison between EE and EI to assess the sensitivity of signal intensity to detect aeration change in the lungs was not reported. We observed that sSI is lower (higher aeration) in the superior portion of the lungs compared with the middle and inferior regions. Although ventilation (gas exchange) is not necessarily equivalent to aeration/air occupancy, interestingly, ventilation has also previously been reported to be nonuniform in the lungs (32–34).

We used sSI of the lungs guided by the high correlations between air occupancy and sSI shown in our phantom experiment. Earlier studies (20,23) illustrated how left and right lung volumes and tidal volumes and left and right hemidiaphragmatic and hemichest wall volume displacements can be measured at dMRI to determine a normative database and to estimate the effects of TIS surgery on the ventilatory pump. The method proposed in this article potentially adds a physiologic component to these assessments, all within a single MRI acquisition, with highly repeatable measurements.

The linear correlation analysis between mean lung sSI and age in healthy children demonstrates that sSI decreases with increasing age (as shown in Fig 5). The relationship between sSI and age for the left lung (at EE and EI) has a greater slope than that for the right lung. This is an interesting finding, although we have not found a similar result in the literature. This suggests that when healthy children are at younger ages, their left lung seems to have higher sSI than their right lung, but the sSI decreases more rapidly with age, such that when the children are at older ages, the left and right lung sSI are closer to each other.

The negative correlations (for sSI and lung volume) changed from −0.41 to −0.64 for healthy children younger than 8 years

but approached zero for healthy children older than 8 years, consistent with prior work on human normal lung growth and alveolar multiplication (28), where alveolar multiplication is most rapid in the first few years of life and appears to slow down and perhaps stop by age 8 years.

One limitation of our study was the relatively small sample size of the group of patients with TIS, which prevented us from performing analyses based on more finely divided age groups of children and separately for male and female individuals. Yet, we were able to compare lung signal intensities between EE and EI for patients with TIS and healthy children and between preoperative and postoperative states in patients with TIS, observing that lung volumes increased and sSIs decreased after surgery. Although in this first attempt we chose to assess aeration properties for the whole left and whole right lungs and in craniocaudal thirds of the lungs, these properties can be further assessed more regionally in the lungs in the future; for example, assessments can be made based on individual lung lobes, as sSI values are available at the voxel level. Such analysis may be helpful in understanding change in aeration as a function of the different types of spinal, chest wall, and diaphragmatic deformities and their corrective procedures.

To our knowledge, this is the first study to demonstrate a practical approach (considering both temporal and spatial resolutions) for lung parenchymal aeration measurement via thoracic dMRI that can be useful for quantifying physiologic changes in healthy children because of maturation, as well as pathophysiologic changes due to TIS and the effects of surgical intervention. Our results show that air occupancy changes are detectable via standardized signal intensity measurement at dMRI, that signal intensity of the lungs at EI is significantly lower than that at EE, and that lung aeration improvement is detectable following surgical intervention in patients with TIS. This method may have great potential for the noninvasive quantitative assessment of regional lung function in other pediatric patient populations, as well as in adult patients with a wide variety of clinical disorders that may affect respiratory function.

Author contributions: Guarantors of integrity of entire study, **Y.T., J.K.U., C.W., L.X.**; study concepts/study design or data acquisition or data analysis/interpretation, all authors; manuscript drafting or manuscript revision for important intellectual content, all authors; approval of final version of submitted manuscript, all authors; agrees to ensure any questions related to the work are appropriately resolved, all authors; literature research, **Y.T., J.K.U., J.M.M., L.X., P.J.C.**; clinical studies, **Y.T., L.X., S.G., O.H.M., J.B.A., D.A.T., P.J.C.**; experimental studies, **Y.T., J.K.U., J.M.M., C.W., L.X.**; statistical analysis, **Y.T., J.K.U., J.M.M., C.W., L.X., S.S.**; and manuscript editing, **Y.T., J.K.U., J.M.M., L.X., C.S.R., O.H.M., J.B.A., D.A.T., P.J.C.**

Disclosures of conflicts of interest: Y.T. No relevant relationships. **J.K.U.** Support for the present article from National Institutes of Health (NIH) grant R01HL150147; patent pending for Quantitative dynamic MRI (QdMRI) analysis and virtual growing child (VGC) systems and methods for treating respiratory anomalies, filed on February 10, 2020, which does not directly cover the topic of this article but is related; co-founder of Quantitative Radiology Solutions, which has created U.S. Food and Drug Administration–approved software for radiation therapy planning, not related to the topic of this article. **J.M.M.** No relevant relationships. **C.W.** No relevant relationships. **L.X.** No relevant relationships. **C.S.R.** No relevant relationships. **S.G.** No relevant relationships. **S.S.** No relevant relationships. **O.H.M.** No relevant relationships. **J.B.A.** No relevant relationships. **D.A.T.** Support for the present article from NIH R01 grant funding; co-founder of Quantitative Radiology Solutions. **P.J.C.** Patent for dynamic lung MRI, which has not been commercialized nor has author received money for it; provisional patent for pediatric deformity system; research grants from the Setting Scoliosis Straight Foundation and the Pediatric Spine Foundation in support of Harms Study Group and the Pediatric Spine Study Group.

References

1. Campbell RM Jr, Smith MD. Thoracic insufficiency syndrome and exotic scoliosis. J Bone Joint Surg Am 2007;89(Suppl 1):108–122.
2. Mayer O, Campbell R, Cahill P, Redding G. Thoracic Insufficiency Syndrome. Curr Probl Pediatr Adolesc Health Care 2016;46(3):72–97.
3. Tsukahara K, Mayer OH. Thoracic insufficiency syndrome: Approaches to assessment and management. Paediatr Respir Rev 2022;44:78–84.
4. Washko GR, Parraga G, Coxson HO. Quantitative pulmonary imaging using computed tomography and magnetic resonance imaging. Respirology 2012;17(3):432–444.
5. Mugler JP 3rd, Altes TA. Hyperpolarized 129Xe MRI of the human lung. J Magn Reson Imaging 2013;37(2):313–331.
6. Fain S, Schiebler ML, McCormack DG, Parraga G. Imaging of lung function using hyperpolarized helium-3 magnetic resonance imaging: Review of current and emerging translational methods and applications. J Magn Reson Imaging 2010;32(6):1398–1408.
7. Capaldi DPI, Eddy RL, Svenningsen S, et al; Canadian Respiratory Research Network. Free-breathing Pulmonary MR Imaging to Quantify Regional Ventilation. Radiology 2018;287(2):693–704.
8. Horn FC, Marshall H, Collier GJ, et al. Regional Ventilation Changes in the Lung: Treatment Response Mapping by Using Hyperpolarized Gas MR Imaging as a Quantitative Biomarker. Radiology 2017;284(3):854–861.
9. Bannier E, Neyran B, Cieslar K, et al. Free breathing hyperpolarized 3He lung ventilation spiral MR imaging. Invest Radiol 2009;44(4):185–191.
10. Levin DL, Chen Q, Zhang M, Edelman RR, Hatabu H. Evaluation of regional pulmonary perfusion using ultrafast magnetic resonance imaging. Magn Reson Med 2001;46(1):166–171.
11. Biederer J, Beer M, Hirsch W, et al. MRI of the lung (2/3). Why … when … how? Insights Imaging 2012;3(4):355–371.
12. Bankier AA, O'Donnell CR, Mai VM, et al. Impact of lung volume on MR signal intensity changes of the lung parenchyma. J Magn Reson Imaging 2004;20(6):961–966.
13. Bauman G, Puderbach M, Deimling M, et al. Non-contrast-enhanced perfusion and ventilation assessment of the human lung by means of fourier decomposition in proton MRI. Magn Reson Med 2009;62(3):656–664.
14. Guo F, Capaldi DPI, McCormack DG, Fenster A, Parraga G. A framework for Fourier-decomposition free-breathing pulmonary 1 H MRI ventilation measurements. Magn Reson Med 2019;81(3):2135–2146.
15. Tibiletti M, Bianchi A, Stiller D, Rasche V. Pulmonary perfusion quantification with flow-sensitive inversion recovery (FAIR) UTE MRI in small animal imaging. NMR Biomed 2016;29(12):1791–1799.
16. Togao O, Tsuji R, Ohno Y, Dimitrov I, Takahashi M. Ultrashort echo time (UTE) MRI of the lung: assessment of tissue density in the lung parenchyma. Magn Reson Med 2010;64(5):1491–1498.
17. Klimeš F, Voskrebenzev A, Gutberlet M, et al. Repeatability of dynamic 3D phase-resolved functional lung (PREFUL) ventilation MR Imaging in patients with chronic obstructive pulmonary disease and healthy volunteers. J Magn Reson Imaging 2021;54(2):618–629.
18. Klimeš F, Voskrebenzev A, Gutberlet M, et al. 3D phase-resolved functional lung ventilation MR imaging in healthy volunteers and patients with chronic pulmonary disease. Magn Reson Med 2021;85(2):912–925.
19. Voskrebenzev A, Kaireit TF, Klimeš F, et al. PREFUL MRI Depicts Dual Bronchodilator Changes in COPD: A Retrospective Analysis of a Randomized Controlled Trial. Radiol Cardiothorac Imaging 2022;4(2):e210147.
20. Hao Y, Udupa JK, Tong Y, et al. OFx: A method of 4D image construction from free-breathing non-gated MRI slice acquisitions of the thorax via optical flux. Med Image Anal 2021;72:102088.
21. Tong Y, Udupa JK, McDonough JM, et al. Quantitative Dynamic Thoracic MRI: Application to Thoracic Insufficiency Syndrome in Pediatric Patients. Radiology 2019;292(1):206–213.
22. Hao Y, Udupa JK, Tong Y, et al. Estimation of the dynamic volume of each lung via rapid limited-slice dynamic MRI. Proc SPIE 2021;11595:115954Y.
23. Tong Y, Udupa JK, McDonough JM, et al. Thoracic quantitative dynamic MRI to understand developmental changes in normal ventilatory dynamics. Chest 2021;159(2):712–723.
24. Tong Y, Udupa JK, McDonough JM, et al. Lung parenchymal characterization via thoracic dynamic MRI in normal children and pediatric patients with TIS. In: Proceedings Volume 11598, Medical Imaging 2021: Image-Guided Procedures, Robotic Interventions, and Modeling. SPIE, 2021;11598.
25. Campbell RM Jr. VEPTR: past experience and the future of VEPTR principles. Eur Spine J 2013;22(Suppl 2):S106–S117.

26. Nyúl LG, Udupa JK. On standardizing the MR image intensity scale. Magn Reson Med 1999;42(6):1072–1081.
27. Xie L, Udupa JK, Tong Y, et al. Automatic lung segmentation in dynamic thoracic MRI using two-stage deep convolutional neural networks. Proc SPIE 2022;12032:120323O.
28. Thurlbeck WM. Lung growth and alveolar multiplication. Pathobiol Annu 1975;5:1–34.
29. Zhang C, Wang Y, Liu L, et al. Regional ventilation distribution in patients with scoliosis assessed by electrical impedance tomography: Is individual thorax shape required? Respir Physiol Neurobiol 2022;299:103854.
30. Burjek NE, Rao KE, Wieser JP, et al. Preoperative Pulmonary Function Test Results Are Not Associated With Postoperative Intubation in Children Undergoing Posterior Spinal Fusion for Scoliosis: A Retrospective Observational Study. Anesth Analg 2019;129(1):184–191.
31. Zapke M, Topf HG, Zenker M, et al. Magnetic resonance lung function--a breakthrough for lung imaging and functional assessment? A phantom study and clinical trial. Respir Res 2006;7(1):106.
32. Frerichs I, Bodenstein M, Dudykevych T, Hinz J, Hahn G, Hellige G. Effect of lower body negative pressure and gravity on regional lung ventilation determined by EIT. Physiol Meas 2005;26(2):S27–S37.
33. Chuong Ngo, Herranz SB, Misgeld B, Vollmer T, Leonhardt S. An object-oriented model of the cardiopulmonary system with emphasis on the gravity effect. Annu Int Conf IEEE Eng Med Biol Soc 2016;2016:2737–2740.
34. Holland J, Milic-Emili J, Macklem PT, Bates DV. Regional distribution of pulmonary ventilation and perfusion in elderly subjects. J Clin Invest 1968;47(1):81–92.
35. Joshi AP, Roth MK, Simmons JW, Shardonofsky F, Campbell RM, Jr. Expansion Thoracoplasty for Thoracic Insufficiency Syndrome Associated with Jarcho-Levin Syndrome. JBJS Essent Surg Tech. 2015;5(2):e12.
36. Mayer OH. Management of thoracic insufficiency syndrome. Curr Opin Pediatr 2009;21(3):333–343.
37. Ramirez N, Flynn JM, Emans JB, Betz R, Smith JT, Price N, St Hilaire T, Joshi AP, Campbell RM. Vertical expandable prosthetic titanium rib as treatment of thoracic insufficiency syndrome in spondylocostal dysplasia. J Pediatr Orthop. 2010;30(6):521-526.
38. Campbell RM Jr, Smith MD, Mayes TC, et al. The characteristics of thoracic insufficiency syndrome associated with fused ribs and congenital scoliosis. J Bone Joint Surg Am 2003;85(3):399–408.
39. Markstaller K, Karmrodt J, Doebrich M, et al. Dynamic computed tomography: a novel technique to study lung aeration and atelectasis formation during experimental CPR. Resuscitation 2002;53(3):307–313.
40. Markstaller K, Eberle B, Kauczor HU, et al. Temporal dynamics of lung aeration determined by dynamic CT in a porcine model of ARDS. Br J Anaesth 2001;87(3):459–468.
41. Higano NS, Fleck RJ, Spielberg DR, et al. Quantification of neonatal lung parenchymal density via ultrashort echo time MRI with comparison to CT. J Magn Reson Imaging 2017;46(4):992–1000.
42. Higano NS, Hahn AD, Tkach JA, et al. Retrospective respiratory self-gating and removal of bulk motion in pulmonary UTE MRI of neonates and adults. Magn Reson Med 2017;77(3):1284–1295.